Al_2O_3 Films Formed by Anodic Oxidation of Al-1 Weight Percent Si-0.5 Weight Percent Cu Films

Re-Long Chiu and Peng-Heng Chang

Institute of Materials Science and Engineering, National Chiao Tung University, Hsinchu, Taiwan 30049

Chih-Hang Tung

Electronics Research and Service Organization, Industrial Technology Research Institute, Chu-Tung, Taiwan 31015

ABSTRACT

The structure of the barrier-type anodic oxide formed on preannealed Al-1 weight percent (w/o) Si-0.5 w/o Cu thin film in a tartaric acid electrolyte was investigated. The oxide film is basically an amorphous layer with a thin dispersed γ'-Al_2O_3 crystalline layer interposed in the center. Pores are observed to be associated with the γ'-Al_2O_3 layer. Silicon nodules and Al_2Cu particles originally present in the Al-1 w/o Si-0.5 w/o Cu film behave differently during anodization. Silicon nodules are oxidized to various degree during anodizing. The silica formed in the Si nodules is amorphous and somewhat porous possibly due to oxygen evolution associated with the Si anodization. A dark rim was found to surround each nodule in the anodic oxide film. This rim is shown to be thicker amorphous Al_2O_3 material, and its origin is attributed to the faster oxidation rate in the vicinity of Si nodules. Al_2Cu precipitates are oxidized to form Al_2O_3 at about the same rate as the surrounding Al matrix. Copper is rejected by Al_2O_3 and accumulates at the Al_2O_3/Al interface.

Introduction

To make large size panels and high resolution thin-film transistors (TFT) for liquid crystal display (LCD), we must choose a metal with low resistivity for the reduction of gate pulse delay and of waveform distortion.[1,2] The resistivity of the gate bus-line metal used in traditional panel displays, such as Cr or Ta, is too high to meet the requirement.[3] The low resistivity and the well-established process technology of Al makes it an attractive choice for this application. However, the propensity of hillocks formation in thin-film Al metal on Si substrate during heat processing, until recently, has prevented their applications in TFT/LCD. Hillocks generally form on Al films to relieve planar compressive stresses introduced either during deposition or subsequently by substrate-induced differential thermal expansion strains.[4] Recently, it was reported[1] that Al anodic oxide film can work as a protective layer against hillock formation. Thin-film transistors with Al gate and an anodic Al_2O_3 + SiN double-layer gate insulator have been applied successfully to the 10.4 in. diagonal multicolor LCD display panel.[1]

The anodic oxidation of Al and its alloys has been studied extensively for applications requiring corrosion resistance, abrasive resistance, electrical insulation, and decorative coloring, etc. Literature is readily available which provides recipes for producing various kinds of anodic aluminum oxide coatings.[5,6] Basically, two types of anodic oxide film can be formed on Al depending on electrolytes used.[5] For solvent electrolytes, such as sulfuric acid, oxalic acid, chromic acid, phosphoric acid, etc., the acid solutions have a solvent effect on the oxide film and thus thick porous oxide films are produced. For nonsolvent electrolytes, *e.g.*, boric acid and tartaric acid, thin impervious oxide films are formed (typically referred to as barrier films[5]). The barrier

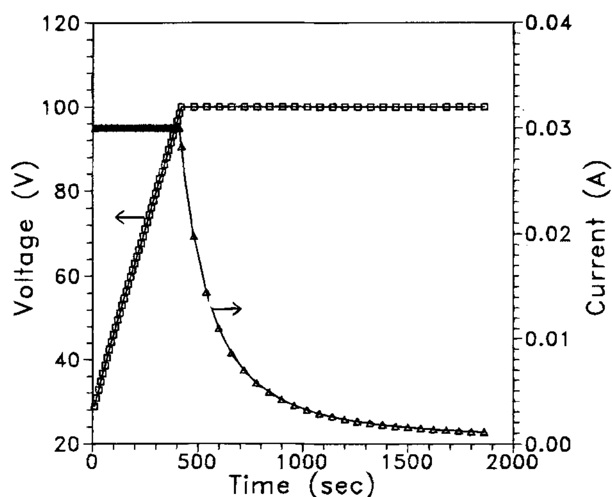

Fig. 1. Variation of potential and current with time during anodizing.

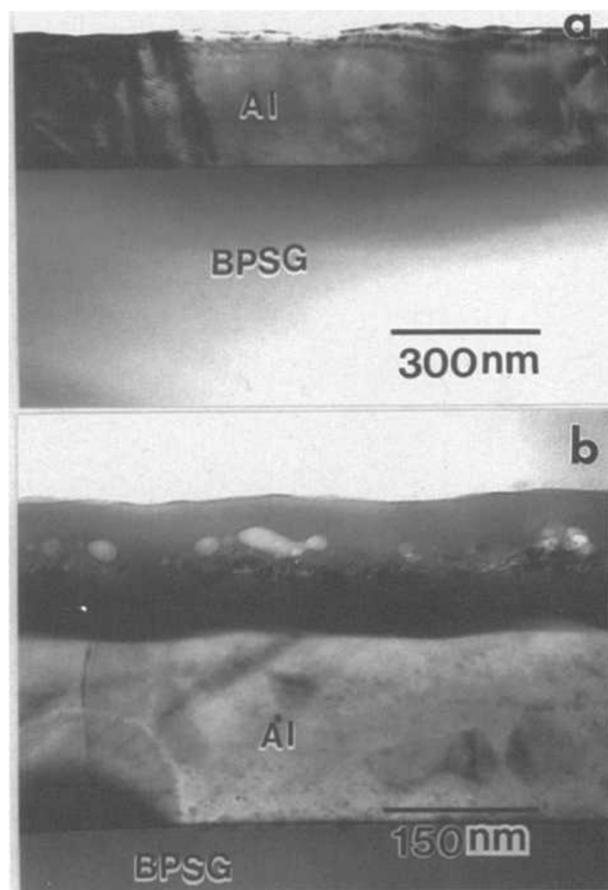

Fig. 2. Cross-sectional TEM micrographs showing the structure of Al-1% Si-0.5% Cu film (a) before anodization treatment and (b) after anodization treatment.

Downloaded on 2014-04-28 to IP 140.113.38.11 address. Redistribution subject to ECS terms of use (see ecsdl.org/site/terms_use) unless CC License in place (see abstract).

film is formed at both film/metal and film/electrolyte interfaces, whereas porous film grows only at the film/metal interface.[7] For integrated circuit (IC) applications, the use of anodic Al_2O_3 is limited mainly to the barrier films. Depending on the anodizing conditions, the anodic oxide film may be either amorphous, crystalline, or a mixture of both.[8-10] The crystal structure of the anodically grown crystalline oxide is a less ordered form of the thermally formed γ-Al_2O_3 and has been designated as γ'-Al_2O_3 in the literature.[10] Both structures have a close-packed oxygen lattice; the differences lie in the degree of ordering in the positions of the aluminum atoms.[10] The degree of crystallinity of the anodic oxide generally increases with decreasing current density and increasing voltage.[9,10] Crystalline film has a higher capacitance because of larger dielectric constant,[10] but it exhibits an electrical instability[11] which are related to the presence of voids[12] and/or to the trapped oxygen.[13] This instability, however, can be removed by a relaxation and reanodization treatment.[11] The crystalline oxide formation is retarded by the anion incorporation from electrolytes.[14] The effect of alloying elements on crystalline oxide formation varies, for example, Mg promotes, but Si and Cu hampers, the γ'-Al_2O_3 formation.[15] Leach and Pearson[16] have correlated the crystallization of various anodic metal oxide to the presence of compressive stress in the film. For anodic aluminum oxide, it is generally agreed that the stress in the film is compressive during anodizing due to electrostriction, but it rapidly changes to tensile in the open-circuit condition.[17-19] Nelson and Oriani[19] have proposed a model which relates the sign and the magnitude of the stress to the Pilling-Bedworth ratio (the ratio of the volume of the oxide formed to the volume of the metal oxidized) of the metal and the transport number of the anion in the oxide. They also showed that the open-circuit stress of anodic aluminum oxide film changes from tensile to compressive when the anodizing current density is $< \sim 0.5$ mA cm^{-2}.

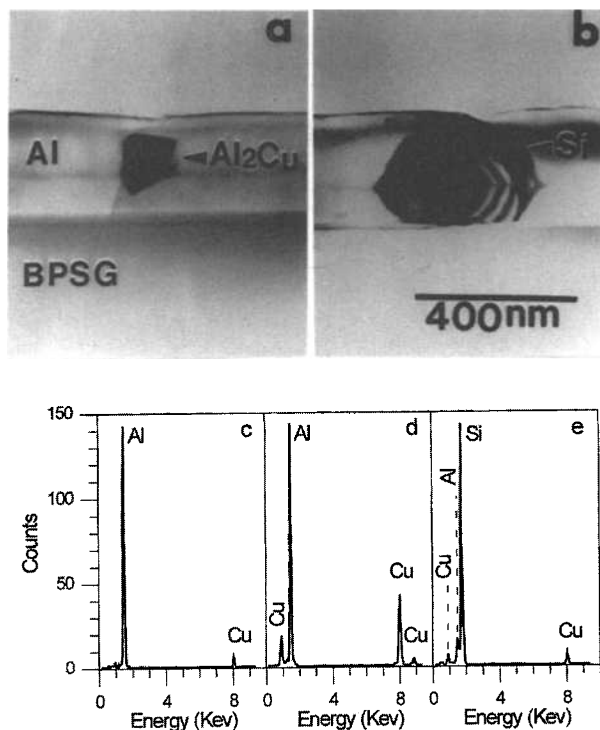

Fig. 4. XTEM micrograph showing (a) Al_2Cu precipitate and (b) Si nodules in aluminum films before anodizing. (c), (d), and (e) are EDX spectra obtained from the Al film matrix, the particle shown in (a), and the particle shown in (b), respectively.

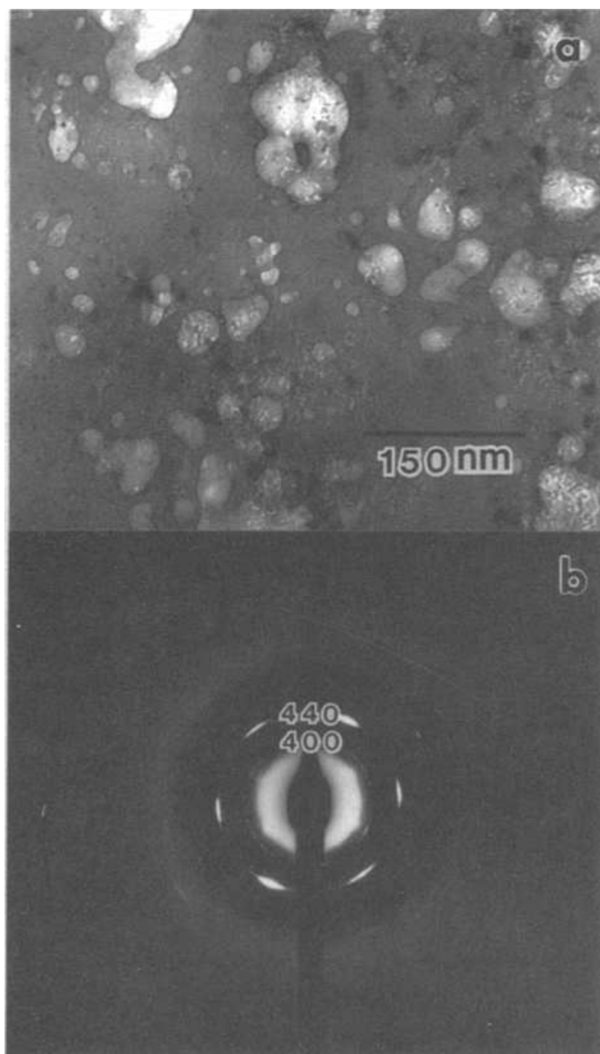

Fig. 3. (a) Planar TEM micrograph showing the structure of the Al_2O_3 film where voids and particles are present. (b) Electron diffraction pattern obtained from the region shown in (a). The ring pattern shows that the particles are γ'-Al_2O_3.

For integrated circuit applications, aluminum metallization is often doped with small amounts of Si and/or Cu to control aluminum spiking[20] and electromigration.[21] Copper-doped Al film has an added advantage of improved resistance to hillock formation.[22] Therefore, it is of great interest to investigate the anodic oxide formed in Al thin films doped with Si and Cu. In this paper, we undertake to study Al_2O_3 layers formed by anodic oxidation of Al-1% Si-0.5% Cu films. Special emphasis is given to the effect of Si and Cu doping on the oxidation behavior.

Experimental

The substrates for this study are 100 mm diam, p-type, <100>, Si wafers. To simulate a typical glass substrate used for LCD display, the Si substrates were first thermally oxidized to form a 550 nm thermal oxide followed by chemical vapor deposition (CVD) of a 600 nm thick borophosphosilicate glass (BPSG) at 720°C. A 300 nm thick Al-Si-Cu film was subsequently deposited in a dc magnetron sputtering deposition machine from an Al-1 w/o Si-0.5 w/o Cu target on top of the BPSG layer. The samples were then annealed in nitrogen for 30 min at 410°C. Al_2O_3 insulating layer was grown by anodizing the Al-Si-Cu layer sputtered on BPSG/SiO_2/Si substrates. Anodization was conducted in AGW electrolyte[23] which is a mixture of 3% aqueous solution of tartaric acid and propylene glycol at a volume ratio of 2 to 8. Constant current mode (current density = 0.4 mA cm^{-2}) was employed initially until the potential reached 100 V, then the experiment was changed to constant voltage mode. The total time of anodization was 30 min and the current density eventually was decreased to 0.015 mA cm^{-2}.

Downloaded on 2014-04-28 to IP 140.113.38.11 address. Redistribution subject to ECS terms of use (see ecsdl.org/site/terms_use) unless CC License in place (see abstract).

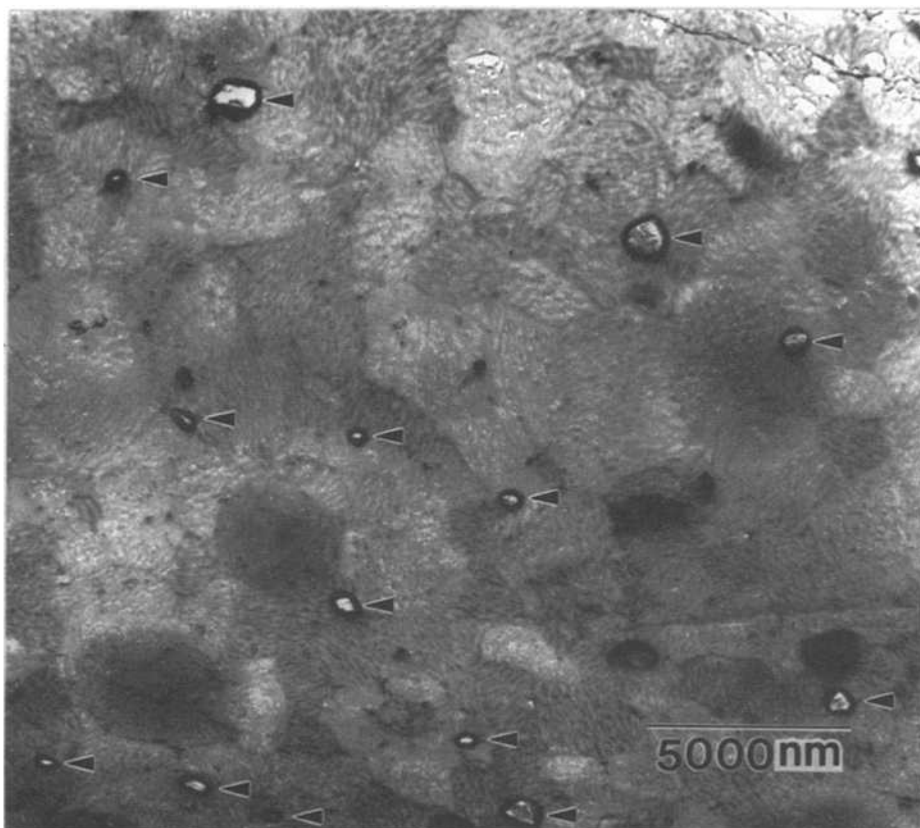

Fig. 5. Planar TEM micrograph of the Al_2O_3 layer near its top surface. Larger rimmed nodules (arrowed) are visible.

Figure 1 shows the variation of voltage and current as a function time from a typical anodizing run.

The structure of the films before and after anodization subsequently was studied by transmission electron microscopy (TEM). Both cross-sectional and planar TEM samples were prepared by ion milling in the usual fashion[24] and examined with a Philips CM20 microscope operating at 160 kV. Energy dispersive x-ray (EDX) analysis was performed using EDAX 9800 with a windowless detector attached to the Philips CM20 microscope. The chemical compositions of the films before and after anodization were profiled by secondary ion mass spectrometry (SIMS) with a VG SIMSLAB 3B using O_2^+ probe at 8 keV, 600 nA.

Results and Discussion

Figure 2a shows a cross-sectional TEM (XTEM) micrograph of the as-deposited Al-Si-Cu film after annealing at 410°C for 30 min and subsequently furnace cooled. Figure 2b shows the oxide layer formed after the 30 min anodic oxidation treatment. The thickness of the as-deposited Al-Si-Cu film is ~300 nm as measured from Fig. 2a. After the anodic oxidation, the thickness of the remaining Al film is ~210 nm while the anodic oxide layer is ~130 nm. Assuming the initial Al thickness is constant across the samples, this means that 90 nm thick Al has been converted to form 130 nm of Al_2O_3, indicating a Pilling-Bedworth ratio of 1.44 which is close to the value reported of crystalline anodic Al_2O_3.[16] Pringle[25] has suggested the use of "nm/V" value (the ratio between the oxide thickness in nanometers and the potential drop across the oxide in volts) as a measure of the resistivity of the oxide. The nm/V value for our anodic oxide is 1.3 which is in excellent agreement with the value of 1.29 reported for a typical anodic aluminum oxide.[25] The anodic oxide film is mostly amorphous but crystalline particles and voids are readily visible near the middle of the amorphous film as clearly revealed in the XTEM micrograph of Fig. 2b. Figure 3a shows a planar view of the anodic oxide film near its center where voids and crystalline particles are present. The white blobs in Fig. 3a correspond to the voids in the middle of the oxide layer shown in Fig. 2b. The voids are typically associated with small dark particles. Selective area diffraction pattern obtained from this region (Fig. 3b) reveals that these particles are γ'-Al_2O_3. From Fig. 3a, the size of the γ'-Al_2O_3 particles is estimated to be less than 30 nm. Voids associated with crystalline Al_2O_3 in the middle of the amorphous Al_2O_3 layer have been observed by many investigators[8,9,26] in anodically formed Al_2O_3 films. The origin of the voids is not clear yet, but two models have been suggested in the literature: (*i*) voids are due to the volume contraction caused by the amorphous to crystalline transformation,[8] or (*ii*) oxygen generated during anodization process tends to be trapped near the crystalline Al_2O_3 particles and eventually results in the formation of voids around them.[9] It has been shown convincingly that the location of the crystalline Al_2O_3 particles corresponds to the original top surface of the Al layer where crystalline nuclei are formed during thermal oxidation.[8,14,26] Subsequent anodization proceeds in a typical ionic transport mechanism[14,25] in which amorphous oxide grows at the oxide/electrolyte and metal/oxide interfaces by the outward migration of metal and inward migration of oxygen, respectively. At appropriate anodizing voltage (which varies with electrolyte), γ'-Al_2O_3 grows on the existing γ-Al_2O_3 nuclei and thus a final amorphous/crystalline/amorphous sandwich structure of Al_2O_3 is developed.

Aluminum films doped with Si and Cu in excess of their solubility limits generally contain precipitates in the form of Si nodules[27] and Al_2Cu particles.[28] These two types of precipitates were observed in the as-deposited Al-Si-Cu films, as shown in Fig. 4. The identification of different phases in a TEM sample is accomplished most easily by EDX, and Fig. 4c-e are EDX spectra obtained from the Al film matrix shown in Fig. 4a, the particle shown in Fig. 4a, and the particle shown in Fig. 4b, respectively. Since the doping level of Si and of Cu is below the detection limit of EDX in our specimens, the weak Cu peak at 8.04 keV in Fig. 4c is due not to the Cu doping in the film but to the sporadic scattering from the Cu supporting ring on which the thin TEM sample is mounted. The coexistence of the strong Al and Cu peaks in Fig. 4d is an indication that the particle shown in Fig. 4a is Al_2Cu. The dominant Si peak in Fig. 4e proves that the particle in Fig. 4b is an Si nodule. It

Downloaded on 2014-04-28 to IP 140.113.38.11 address. Redistribution subject to ECS terms of use (see ecsdl.org/site/terms_use) unless CC License in place (see abstract).

is of great interest to investigate the behavior of these precipitates during anodizing. Figure 5 is a planar TEM micrograph of the anodic film in which many large white nodules (marked by arrows), each with a dark rim around it, are randomly distributed in the film. Figure 6a shows a blowup of a large nodular precipitate similar to the ones shown in Fig. 5. To take this micrograph, the specimen purposely was tilted to a major zone axis so that the inner region is in strong diffraction contrast. The inner region in Fig. 6a consists of mostly a dark area, but small lighter areas clearly can be seen to surround it. Figure 6b is an electron diffraction pattern corresponding to the dark inner region. The spot pattern in this figure can be ascribed unambiguously to the [111] zone axis of Si while the faint ring pattern is due to the underlying unreacted Al substrate. This proves that the dark region is crystalline Si. The lighter regions which do not show any diffraction con-

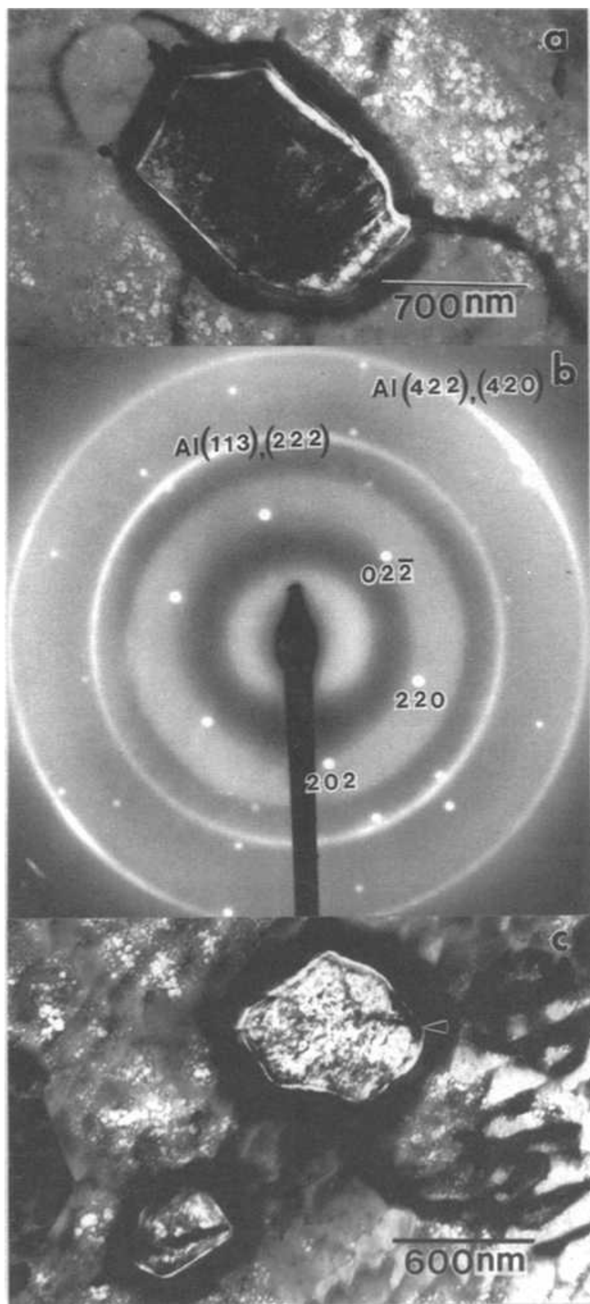

Fig. 6. (a) Blowup view of the rimmed nodules shown in Fig. 5. (b) Electron diffraction pattern obtained from the dark inner region of (a), the spot pattern is due to Si [$\bar{1}$11] zone and the faint ring pattern is due to the underlying unreacted Al layer. (c) Another rimmed nodule with most of its Si content oxidized.

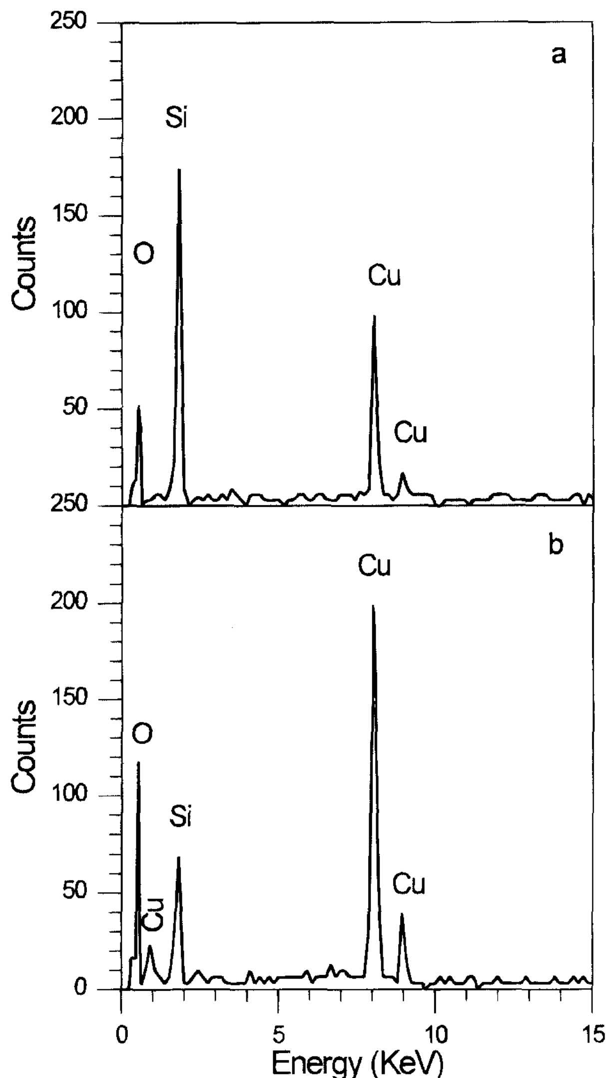

Fig. 7. EDX spectra from (a) the dark region inside the rimmed nodule of Fig. 6a, and (b) the lighter region inside the rimmed nodule of Fig. 6c.

trast are most likely amorphous in nature. The relative amount of the dark and lighter regions in the rimmed nodular precipitates varies significantly. Figure 6c shows a similar precipitate in which the inner region is composed mostly of a light amorphous phase, but a small dark patch of material (marked by arrow) can be observed at the upper right. This dark patch is identified as Si by electron diffraction. To identify the lighter amorphous phase we resorted to the EDX technique. Figures 7a and b are the EDX spectra obtained from the dark region in Fig. 6a and the lighter region in Fig. 6c, respectively. The Cu peaks which are present in all the EDX spectra here are mostly artifacts from the TEM sample holder. No Al signal is detected in these regions. Consistent with the electron diffraction result shown in Fig. 6b, the major strong peak in Fig. 7a is due to Si, indicating the dark area is primarily Si. The small oxygen peak in Fig. 7a is indicative of the presence of a small amount of silicon oxide. The spectrum in Fig. 7b also consists of Si and oxygen peaks, but the oxygen peak intensity is much higher than that of the Si peak. This implies that the region is made mostly of silicon oxide. Based on the electron diffraction and EDX results we conclude that the rimmed nodular precipitates in the anodic oxide film are Si nodules oxidized to various degrees. The standard free-energy of formation is higher for SiO_2 than for Al_2O_3,[29] so Al matrix is oxidized prior to Si nodules during anodization. But the indiffusing oxygen eventually oxidizes the Si nodules at different depths to various degrees, thus forming nodules consisting of mixtures of crystalline Si and silicon

Downloaded on 2014-04-28 to IP 140.113.38.11 address. Redistribution subject to ECS terms of use (see ecsdl.org/site/terms_use) unless CC License in place (see abstract).

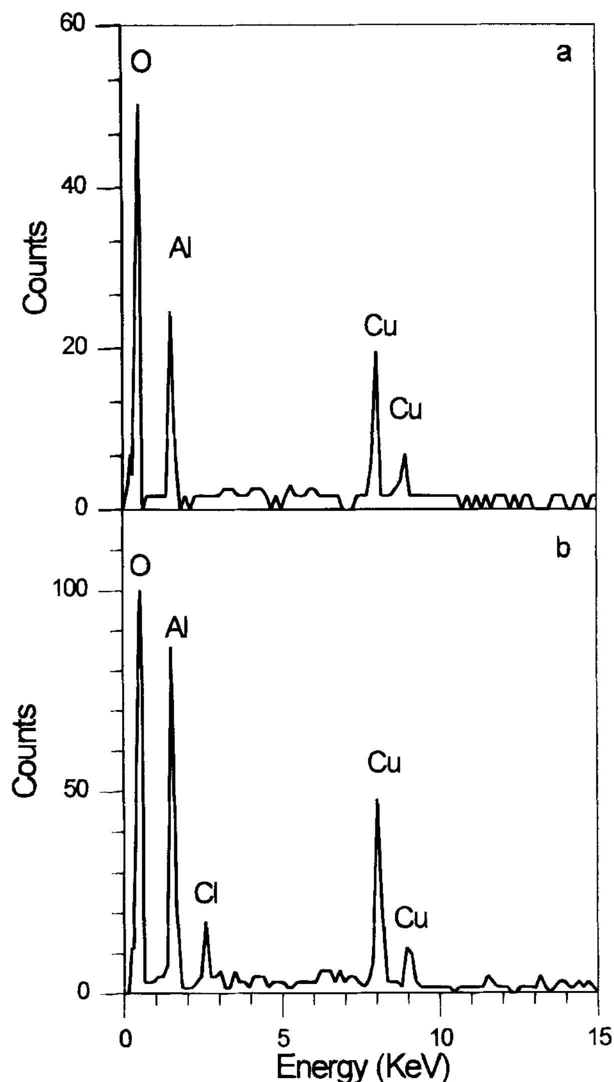

Fig. 8. EDX spectra from (a) the dark rim of the rimmed nodule and (b) the neighboring Al_2O_3 matrix.

oxide of various proportions such as those observed in Fig. 6a and c.

The nature of the dark rims surrounding the Si/silica nodules is more difficult to analyze. Despite numerous attempts, no electron diffraction pattern could be obtained from the dark rim region, indicating that it is probably amorphous. (To substantiate this conjecture we point out that no diffraction contrast was ever observed in the dark rim region either.) EDX analysis was conducted on the rim region in the hope of getting some ideas about its chemistry, and a typical spectrum is shown in Fig. 8a. We see from the spectrum that the major constituents of the rim region are

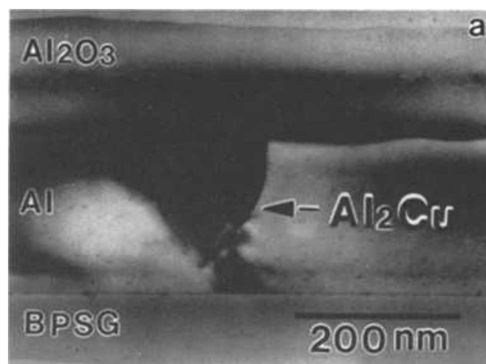

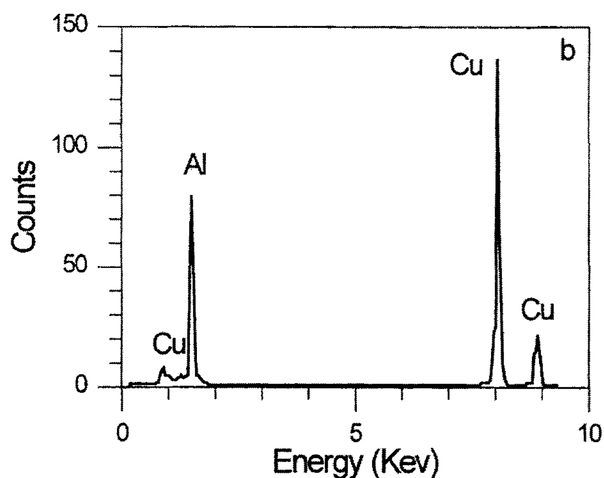

Fig. 10. (a) XTEM micrograph showing Al_2O_3 film cutting through an Al_2Cu precipitate originally present in the aluminum film. (b) The EDX spectrum obtained from the Al_2Cu precipitate shown in (a).

Al and oxygen. For comparison, an EDX spectrum from the neighboring Al_2O_3 matrix is shown in Fig. 8b. The two spectra are similar except that the oxygen content seems to be higher in the rim region than in the matrix (the extra Cl peak at 2.62 keV in Fig. 8b probably is due to contamination of the TEM sample during handing). These results strongly suggest that the dark rim is also aluminum oxide. Figure 9 shows an XTEM micrograph of a rimmed particle in the Al_2O_3 layer. This particle was originally an Si nodule ~0.65 μm in size which was located at the film surface initially. The top portion of the nodule apparently has been

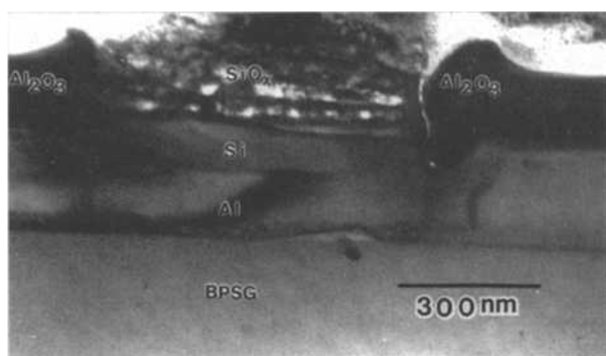

Fig. 9. XTEM micrograph showing a rimmed nodule in the Al_2O_3 film.

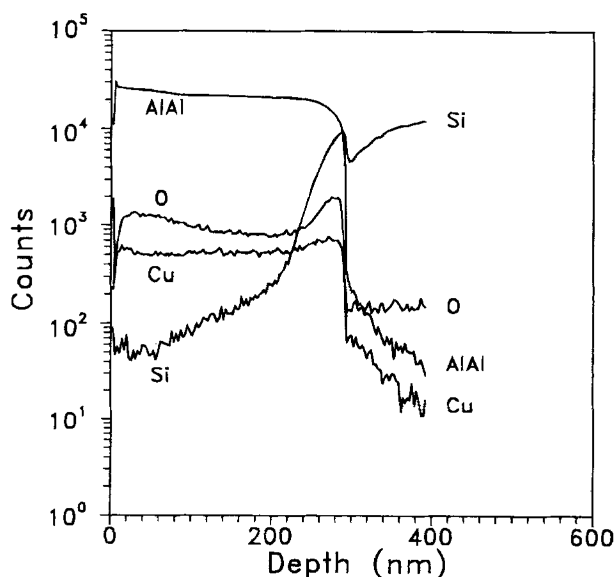

Fig. 11. SIMS profile of the sample before anodization.

Downloaded on 2014-04-28 to IP 140.113.38.11 address. Redistribution subject to ECS terms of use (see ecsdl.org/site/terms_use) unless CC License in place (see abstract).

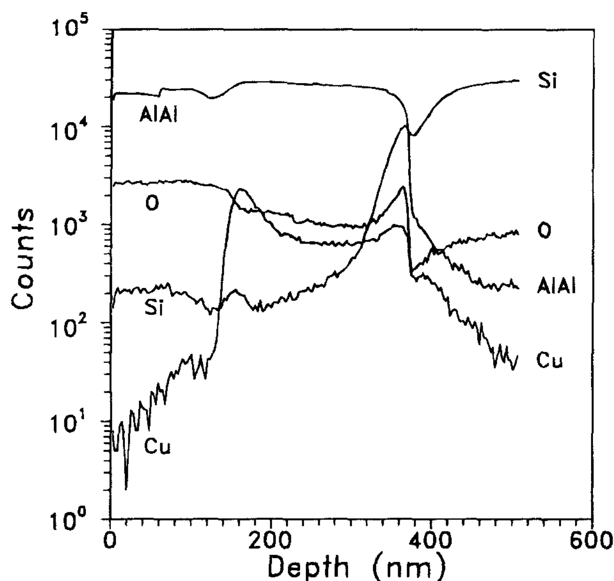

Fig. 12. SIMS profile of the sample after anodization.

oxidized to a porous and amorphous silica structure while its bottom remains crystalline Si. The thickness of the Al_2O_3 layer at the vicinity of the particle is much larger than regions away from the particle, thus forming an Al_2O_3 spike around the particle. On comparing the morphology of the rimmed particle shown in Fig. 9 to the one shown in Fig. 6a, it is apparent that the rim is also Al_2O_3 and it appears to be darker because of its larger thickness. Rimmed Si nodules oxidized to various degrees have been observed by Shimizu *et al.*[30] in bulk binary Al-1.5% Si alloy anodized in 0.1*M* ammonium borate solution. Thicker Al_2O_3 film growth in regions surrounding the Si particle also was observed and was ascribed to the local current concentration effects (such as heating) at the Si particle during anodizing.[30] The porous nature of the amorphous silica observed here likely is due to the oxygen evolution during the oxidation of Si nodules, a phenomenon reported in the anodizing of Al alloys containing 8.5 to 10% Si in a 5 w/o ammonium pentaborate solution.[31] Due to their cross-sectional TEM sample preparation technique (which is performed by ultramicrotomed sectioning in contrast to ion milling used here), Shimizu *et al.*[30] were uncertain about the nature of the dark rims and thought that they may "merely reflect some artifact developed during sectioning." Since ion milling is much less prone to artifacts than ultramicrotomed sectioning, the present result in a way confirms unequivocally the presence of thicker oxide rims around Si nodules.

Al_2Cu precipitates behaved in a totally different way from that of Si nodules during anodizing. Figure 10a shows an anodic oxide, ~140 nm thick, formed on top of the Al-Si-Cu layer. The EDX spectrum in Fig. 10b is obtained from the black particle in the Al layer, and the strong Al and Cu peaks in this spectrum are a clear indication that the particle is an Al_2Cu precipitate. This Al_2Cu particle is originally present in the Al-Si-Cu film prior to anodization, but is cut through by the advancing oxide film. From the morphology of the Al_2Cu particle it is apparent that the top portion of it has been oxidized. The TEM structure of the anodic oxide directly on top of the Al_2Cu particle is not different from the oxide material which is directly on top of Al. Also, the Al_2O_3/Al interface is smooth across the Al_2Cu particle. These results seem to indicate that the oxidation rate is comparable for the Al-1% Si-0.5% Cu matrix and the Al_2Cu precipitates in our films. By EDX, we have checked the bulk chemistry of the Al_2O_3 material directly on top of the precipitate and found no significant difference from regions directly on top of the Al. The oxide film directly on top of the Al_2Cu particle is not enriched in Cu. Further insight of the change in film chemistry due to anodization can be obtained from SIMS analysis. Figures 11 and 12 show, respectively, the composition profiles of the films before and after anodizing. The Al/BPSG interface is at ~290 nm in Fig. 11 for the film before anodizing. After anodizing, this interface is moved to a depth of 390 nm, see Fig. 12, due to the volume expansion associated with the oxide formation. The Al_2O_3/Al interface in Fig. 12 is located at ~150 nm. From these two figures we see that the Al and Si signals do not have any significant change as a result of anodization. The high level of O signal in the Al film shown in Fig. 11 (comparable with the oxygen level shown in the Al_2O_3 film in Fig. 12) does not mean that the as-deposited film contains a high concentration of oxygen. It is just an artifact due to the use of an oxygen probe for the depth profiling. The Cu signal in the anodic oxide layer is apparently one to two orders of magnitude lower than the Cu signal in the remaining unreacted Al layer as shown in Fig. 12. A notable Cu peak is observed also at the Al_2O_3/Al interface. These results strongly suggest that the solubility of Cu in Al_2O_3 is lower than in Al. Copper is rejected by Al_2O_3 and builds up at the interface during anodization. It is likely that when the advancing Al_2O_3/Al interface encounters an Al_2Cu precipitate during anodization, dissociation of Al_2Cu to Al and Cu occurs first; and Al subsequently is converted to Al_2O_3 while Cu is rejected to the interface. The rejection of Cu by the anodic aluminum oxide and the accumulation of Cu at the Al_2O_3/Al interface have been observed previously by Strehblow *et al.*[32] in sputter deposited Al-Cu films using Rutherford backscattering spectrometry (RBS). These authors have speculated that the formation of copper-enriched metal intrudes into the oxide phase leading to the breakdown of the anodic film, but this hypothesis is not supported by our TEM observation which shows a flat interface even at the vicinity of an Al_2Cu precipitate. Although there is Cu accumulation at the oxide/metal interface, the cross-sectional TEM results clearly rule out the existence of any identifiable phase due to the excess Cu concentration.

Conclusion

The anodic oxide formed on Al-1% Si-0.5% Cu thin film is basically an amorphous layer with a thin γ'-Al_2O_3 crystalline layer interposed in the center. Pores are observed to be associated with the γ'-Al_2O_3 layer. The 410°C preannealed Al films contain precipitates of Al_2Cu particles and Si nodules. Silicon nodules are oxidized to various degrees during anodizing. The silica formed in the Si nodules is amorphous and a dark rim surrounded each nodule. The dark rim is thicker amorphous Al_2O_3 material, and its origin is attributed to the faster oxidation rate in the vicinity of Si nodules. The faster oxidation rate probably is due to the localized Joule heating caused by the local current concentration induced by the presence of Si nodules. The silica structure is somewhat porous which can be explained by the oxygen evolution associated with the anodization of Si. Al_2Cu precipitates are oxidized to form Al_2O_3 at about the same rate as the surrounding Al matrix. Copper oxide is not detected in the anodic Al_2O_3 films. The solubility of Cu in Al_2O_3 is lower than that in Al so that copper is rejected by Al_2O_3 and accumulates at the Al_2O_3/Al interface.

Acknowledgment

This work was supported in part by the National Science Council, Taiwan, Republic of China, through Grant No. NSC 83-0404-E-009-098. We express our appreciation to one of the reviewers who directed our attention to the work of Strehblow *et al.* on Al-Cu films.

Manuscript submitted Jan. 28, 1994; revised manuscript received Sept. 7, 1994.

National Chiao Tung University assisted in meeting the publication costs of this article.

REFERENCES

1. H. Yamamoto, H. Matsumaru, K. Shirahashi, M. Nakatani, A. Sasano, N. Konishi, K. Tsutsui, and T. Tsukada, *1990 Int. Electron Device Meet., Techn. Digest,* 851 (1990).

Downloaded on 2014-04-28 to IP 140.113.38.11 address. Redistribution subject to ECS terms of use (see ecsdl.org/site/terms_use) unless CC License in place (see abstract).

2. T. Sunata, T. Yukawa, K. Miyake, Y. Matsushita, Y. Murakami, Y. Ugai, J. Tamamura, and S. Aoki, *IEEE Trans. Electron Devices,* **ED-33,** 1212 (1986).
3. W. J. Sah, J. L. Lin, and S. C. Lee, *ibid.,* **ED-38,** 676 (1991).
4. C. Y. Chang and R. W. Vook, *Thin Solid Films,* **228,** 205 (1993).
5. V. F. Henley, *Anodic Oxidation of Aluminum & Its Alloys,* Pergamon Press, Oxford (1982).
6. S. Wernick, R. Pinner, and P. G. Sheasby, *The Surface Treatment and Finishing of Aluminum and Its Alloys,* 5th ed., Finishing Publ. Ltd., Teddington, England (1987).
7. S. Sato, H. Ichinose, and N. Masuko, *This Journal,* **138,** 3705 (1991).
8. K. Kobayashi and K. Shimizu, in *Aluminum Surface Treatment Technology,* R. S. Alwitt and G. E. Thompson, Editors, PV 86-11, p. 380, The Electrochemical Society Proceedings Series, Pennington, NJ (1986).
9. C. Crevecoeurs and H. J. de Wit, *This Journal,* **134,** 808 (1987).
10. C. T. Chen and G. A. Hutchins, *ibid.,* **132,** 1567 (1985).
11. R. S. Alwitt and C. K. Dyer, *Electrochim. Acta,* **23,** 355 (1978).
12. R. S. Alwitt, C. K. Dyer, and B. Noble, *This Journal,* **129,** 711 (1982).
13. W. J. Bernard and P. G. Russell, *ibid.,* **127,** 1256 (1980).
14. G. E. Thompson and G. C. Wood, in *Treatise on Materials Science and Technology,* Vol. 23, J. C. Scully, Editor, p. 205, Academic Press, London (1983).
15. M. J. Dignam, *This Journal,* **109,** 184 (1962).
16. J. S. Leach and B. R. Pearson, *Corros. Sci.,* **26,** 43 (1988).
17. R. S. Alwitt, J. Xu, and R. C. McClung, *This Journal,* **140,** 1241 (1993).
18. N. Wuthrich, *Electrochim. Acta,* **26,** 1617 (1981).
19. J. C. Nelson and R. A. Oriani, *Corros. Sci.,* **34,** 309 (1993).
20. P. H. Chang, R. Hawkins, T. D. Bonifield, and L. A. Melton, *Appl. Phys. Lett.,* **52,** 272 (1988).
21. P. B. Ghate, in *Proceedings of the IEEE International Reliability Physics Symposium,* p. 243 (1981).
22. S. Wolf and R. N. Tauber, *Silicon Processing for the VLSI Era,* Vol. 2, p. 271, Lattice Press, California (1990).
23. H. Hasegawa and H. L. Hartnagel, *This Journal,* **123,** 713 (1976).
24. P. H. Chang, H. Y. Liu, J. A. Keenen, and J. M. Anthony, *J. Appl. Phys.,* **62,** 2485 (1987).
25. J. P. Pringle, *Electrochim. Acta,* **25,** 1423 (1980).
26. K. Kobayashi and K. Shimizu, *This Journal,* **135,** 908 (1988).
27. C. H. Tung, C. T. Chang, H. C. Chang, S. Chiu, B. Kou, and L. S. Chang, *J. Appl. Phys.,* **68,** 1592 (1990).
28. D. R. Frear, J. E. Sanchez, A. D. Romig, Jr., and J. W. Morris, Jr., *Met. Trans.,* **A21,** 2449 (1991).
29. L. S. Darken and R. W. Gurry, *Physical Chemistry of Metals,* p. 349, McGraw-Hill Book Co., New York (1953).
30. K. Shimizu, G. E. Thompson, and G. C. Wood, *Electrochim. Acta,* **27,** 245 (1982).
31. H. S. Kim, G. E. Thompson, G. C. Wood, I. G. Wright, and R. E. Marringer, *Trans. Inst. Met. Finish.,* **62,** part 2, 49 (1984).
32. H.-H. Strehblow, C. M. Melliar-Smith, and W. M. Augustyniak, *This Journal,* **125,** 915 (1978).

Downloaded on 2014-04-28 to IP 140.113.38.11 address. Redistribution subject to ECS terms of use (see ecsdl.org/site/terms_use) unless CC License in place (see abstract).